Title: $BaCo_{0.4}Fe_{0.4}Zr_{0.1}Y_{0.1}O_{3-\sigma}$ Cathode Performance for Proton Conducting Solid Oxide Fuel Cells with $BaZr_{0.8-x}Ce_xY_{0.1}Yb_{0.1}O_{3-\delta}$ Electrolytes

Author Names: *Wenhao Li [a,b], Md Shariful Islam Sozal [a,b], Vadym Drozd [b], Andriy Durygin [b], Zhe Cheng [a,b] **
Affiliation(s):
[a] *Department of Mechanical and Materials Engineering, Florida International University, Miami, FL, 33174, USA.*
[b] *Center for the Study of Matter at Extreme Conditions (CeSMEC), Florida International University, Miami, FL, 33199, USA.*
Corresponding Author: zhcheng@fiu.edu

Abstract Text
$BaCo_{0.4}Fe_{0.4}Zr_{0.1}Y_{0.1}O_{3-\sigma}$ (BCFZY) is a proton, oxygen-ion, and electron-hole conducting cathode material for intermediate temperature solid oxide fuel cells. Its electrode reaction mechanism in air with moisture is not well understood. In this study, three types of symmetrical cells with the same BCFZY cathode were fabricated over three related proton conducting electrolytes: $BaZr_{0.8-x}Ce_xY_{0.1}Yb_{0.1}O_{3-\delta}$ (x = 0.1, 0.4, and 0.7). The cathode shows similar performance over three different electrolytes in dry air but different responses to moisture introduction. The differences are hypothesized to relate to the mutual diffusion at the cathode/electrolyte interface. Such a hypothesis is supported by different techniques such as XRD Rietveld refinement of BCFZY cathode in mixtures with different electrolytes after firing, energy-dispersive X-ray spectroscopy (EDS) line scanning for element concentration distribution at the cathode/electrolyte interface, as well as electrochemical test for a related BaCoFeO-type cathode with Zr replaced by Ce.

Introduction

Proton conducting solid oxide fuel cells (PC-SOFC) with intermediate operating temperature (400-600 ºC) have great potential in clean power generation[1,2]. Compared with traditional oxygen ion conducting solid oxide fuel cells (OC-SOFC), PC-SOFC has advantages such as lower activation energy, better tolerance to sulfur and less energy loss during operation[3–6]. For PC-SOFC, Ba-based perovskite oxides are often used as the electrolyte because they have better ionic conductivity compare with electrolytes used in OC-SOFC at ~400-600 ºC[7–9]. Among $BaZr_{0.8-x}Ce_xY_{0.1}Yb_{0.1}O_{3-\delta}$ (BZCYYb) series of electrolytes, $BaZr_{0.1}Ce_{0.7}Y_{0.1}Yb_{0.1}O_{3-\delta}$ (Ce-rich) is commonly used due to its high conductivity, but it suffers from low stability[10–12]; $BaZr_{0.7}Ce_{0.1}Y_{0.1}Yb_{0.1}O_{3-\delta}$ (Zr-rich) offers high stability, but is difficult to process and much less conductive. In comparison, $BaZr_{0.4}Ce_{0.4}Y_{0.1}Yb_{0.1}O_{3-\delta}$ (ZrCe-bal) has received more attention in recent years for its balanced properties[13].

On the other hand, for PC-SOFC, previous studies show that mixing conventional mixed ionic electronic cathode (MIEC) materials such as $La_{0.4}Sr_{0.6}Co_{0.2}Fe_{0.8}O_{3-\sigma}$ (LSCF) and $SrCo_{0.8}Nb_{0.1}Ta_{0.1}O_{3-\delta}$ (SCNT) with proton conducting electrolyte leads to better performance[14,15]. But the reaction site for such composite cathode is still confined to the air/electrode/electrolyte triple phase boundary (TPB), potentially limiting cell performance. In comparison, triple (i.e., electron, oxygen ion, and proton) conducting cathode have

attracted attention recently[13,16], because the entire surface can be active as the reaction sites, removing the limitation by TPB length[17,18]. However, critical aspects for triple conducting cathodes for such PC-SOFC remain unknown. For example, the cathode/electrolyte chemical interaction and the relationship between electrolyte conductivity and electrode performance are not all clear. In addition, the influence of moisture on such triple conducting cathode is also not well characterized. Therefore, in this research, $BaCo_{0.4}Fe_{0.4}Zr_{0.1}Y_{0.1}O_{3-\delta}$ (BCFZY) is used as an example triple conducting cathode to study these unknowns. BCFZY is a promising cathode enabling high PC-SOFC performance[1]. The interactions of BCFZY cathode with the three representative BZCYYb electrolytes (i.e., Ce-rich, Zr-rich, ZrCe-bal) are studied using XRD and EDS. The electrochemical behaviors for BCFZY cathode symmetrical cells over the three electrolytes in different atmospheres are reported. Possible explanation for the different electrochemical behaviors is hypothesized and supported by tests using a new BaCeFeO-type cathode - $BaCo_{0.4}Fe_{0.4}Ce_{0.1}Y_{0.1}O_{3-\delta}$ (BCFCY) that replaces Zr in the cathode with Ce.

Experimental

Powder synthesis and compatibility test

All of the BZCYYb electrolyte powder, such as $BaZr_{0.1}Ce_{0.7}Y_{0.1}Yb_{0.1}O_{3-\delta}$ (Ce-rich), $BaZr_{0.4}Ce_{0.4}Y_{0.1}Yb_{0.1}O_{3-\delta}$ (ZrCe-bal), $BaZr_{0.7}Ce_{0.1}Y_{0.1}Yb_{0.1}O_{3-\delta}$ (Zr-rich), and $BaCo_{0.4}Fe_{0.4}Zr_{0.1}Y_{0.1}O_{3-\delta}$ (BCFZY) as well as $BaCo_{0.4}Fe_{0.4}Ce_{0.1}Y_{0.1}O_{3-\delta}$ (BCFCY) cathode materials were synthesized by Pechini method.[19] The metal salts contain $Ba(NO_3)_2$ (#A11305, Alfa Aesar, 99%), $ZrO(NO_3)\cdot 12H_2O$ (#43224, Alfa Aesar, 99.9%), $Ce(NO_3)_3\cdot 6H_2O$ (#11329, Alfa Aesar, 99.5%), $Y(NO_3)_3\cdot 6H_2O$ (#12898, Alfa Aesar, 99.9%), $Yb(NO_3)_3\cdot 6H_2O$ (#12901,Alfa Aesar,99.9%), $Co(NO_3)_3.6H_2O$ (#239267,Sigma Aldrich,>=98%), $Fe(NO_3)_3\cdot 9H_2O$ (#216828-500G,Sigma Aldrich,>=98%). After dissolving the metal salt in deionized (DI) water in a 2 L glass beaker according to the designed stoichiometric ratio, citric acid monohydrate (#22869, Alfa Aesar, 99.5+%, Hygroscopic) and ethylene glycol (Alfa Aesar, A 17925) were added to the beaker with the molar ratio of total metal ion : citric acid : ethylene glycol of 1 : 1.5 : 1.5. The mixed solutions in glass beakers were heated up on a hot plate set at ~540 ºC. After the water was completely evaporated, porous precursors were obtained. All precursors were cooled and hand ground into powder for the final calcination step. The three electrolytes (Ce-rich, ZrCe-bal, Zr-rich) were all calcined at 1300 ºC for 5 h in air to obtain the pure phases. BCFZY cathode needs heat treatment at 1000 ºC for 5 h to form the pure phase, while BCFCY cathode needs 1200 ºC for 5 h to remove impurities and obtain the same phase as BCFZY. The ramp rates of all calcination were 5 ºC/min for heating and cooling.

To study the chemical compatibility and mutual diffusion between the three BZCYYb-type electrolytes and the BCFZY cathode, the powders of each electrolyte and the BCFZY cathode were mixed at the weight ratio of 1:1 and went through the same firing process as symmetrical cell cathode fabrication, which was 4 h at 1100 ºC. The as-synthesized powders and the mixed powders after firing were analyzed by X-ray diffraction (XRD, Rigaku BD700535-01, Cu-K_α radiation, λ = 1.541874 Å) for phase composition.

Thermogravimetric analysis (TGA)

TGA was used to measure the weight change of each electrolyte powder in dry air. To obtain more accurate data, a two-cycle TGA was performed: in the first cycle, the sample was heated up to 800 ºC at 5 ºC/min and held for 1 h to fully remove the adsorbed water before cooling it down to room temperature. In the second cycle, the same sample from the first one was again heated to 800 ºC at 5 ºC/min and cooled down to room temperature. The final weight at the end of the first cycle would be the starting weight for the second cycle. The change of oxygen contents for the BZCYYb electrolytes with temperature can be obtained based on TGA from the second cycle[13], by assuming the room temperature oxygen contents of the three electrolytes (Ce-rich, ZrCe-bal, Zr-rich) as 2.9. Such an assumption was supported by XRD Rietveld refinement and was also consistent with iodometric titration measurement in the literature[20].

Symmetrical cells fabrication and microstructure examination

For pellet fabrication, all electrolytes were sintered following the same process. Using $BaZr_{0.1}Ce_{0.7}Y_{0.1}Yb_{0.1}O_{3-\delta}$ (Ce-rich) electrolyte as an example, the Ce-rich powder was mixed with 0.5wt% NiO as the sintering aid by hand grounding. 0.2 g mixed powder was dry pressed under ~300 MPa into a 10 mm pellet pressing die. The prepared green pellets were sintered at 1450 ºC for 10 h in air in a muffle furnace to form dense pellets. In order to reduce Ba loss[21] and unexpected reaction with Al crucible, the pellets were vertically stacked, separated and surrounded by the corresponding electrolyte powder. The electrode slurries were made by mixing the cathode powder (e.g., either BCFZY or BCFCY that has all Zr replaced by Ce) and 4 wt.% ethyl cellulose (EC) dissolved in alpha-terpineol with the weight ratio of 3:7 (e.g., 0.6 g of BCFZY powder and 1.4 g of 4 wt.% EC in alpha-terpineol). Then the slurry was brush painted on both sides of the electrolyte pellet with an active area ~0.16 cm^2 and calcinated at 1100 ºC for 4 h in air in a muffle furnace at a lower ramp rate of 2.5 ºC/min for both the heating and cooling process to obtain the symmetrical cell. The microstructure of the surface of three electrolytes and the cross section of the symmetrical cell were analyzed by a scanning electron microscope (SEM JEOL JSM-F100) fitted with energy dispersive X-ray spectroscopy (EDS).

Electrochemical measurements

Electrochemical impedance spectroscopy (EIS) measurements were performed on symmetrical cells under open circuit conditions using a potentiostat (Gamry Interface 1000) in the frequency range 10^6 to 0.01 Hz with an AC amplitude of 1 mA. Fritless silver paste was brushed onto the electrodes of the symmetrical cell to collect current. The cell was placed in a sealed tube furnace (OTF-1200), heated to 750 ºC and stabilized over 12 h before EIS testing. Each symmetrical cell was first tested in dry simulated air (Ultra Zero Grade, Airgas, with <5 ppm H_2O and CO_2 by volume). The EIS data was collected every 50 ºC from 650 ºC to 450 ºC with an air flow of 40 cc min^{-1}. To test the effect of H_2O, the cell was heated up again to 650 ºC and 3% H_2O was introduced (by passing the simulated air through a water bubbler). After holding for over 24 h, the cell hydration effect would saturate and the cell was then tested from 650 ºC to 450 ºC by EIS to compare the electrochemical behaviors in moist air vs. simulated (dry) air.

Results & Discussion

Phase identification for as-synthesized electrolytes and cathodes

Fig. 1(a) shows the XRD patterns of the three electrolyte powders $BaZr_{0.1}Ce_{0.7}Y_{0.1}Yb_{0.1}O_{3-\delta}$ (Ce-rich), $BaZr_{0.4}Ce_{0.4}Y_{0.1}Yb_{0.1}O_{3-\delta}$ (ZrCe-bal), and $BaZr_{0.7}Ce_{0.1}Y_{0.1}Yb_{0.1}O_{3-\delta}$ (Zr-rich) after heat treatment at 1300 ºC for 5 h. The result indicates that all electrolytes are pure phase perovskites and the peaks shift to the right or higher 2θ angle with higher Zr concentrations. This is because the Zr ion is smaller than the Ce ion. Fig.1(b) shows the XRD Rietveld refinement of the Ce-rich electrolyte, indicating that it has an orthorhombic Pnma space group with lattice parameters of a = 6.195 Å, b = 8.695 Å, c = 6.201 Å (4 formula per unit cell? Equivalent pseudo-cubic lattice parameter = 4.3709 Å). With lower Ce concentration, the crystal structure of the electrolyte becomes cubic: Fig. 1(c) shows the refinement for the ZrCe-bal electrolyte, illustrating that it has a cubic $Pm\bar{3}m$ space group with a lattice parameter of a = 4.311 Å. The refinement of the Zr-rich electrolyte is shown in Fig. 1(d). It also has the cubic $Pm\bar{3}m$ space group with an even smaller lattice parameter of 4.216 Å. The refinement R_{wp} values of these electrolytes are 9.43%, 8.80% and 9.68%, respectively, indicating the calculated data match well with the XRD patterns. The trend in lattice volume (or (equivalent) lattice parameters) also matches with the shift in obtained XRD patterns.

Fig. 2(a) shows the XRD patterns of the as-synthesized $BaCo_{0.4}Fe_{0.4}Zr_{0.1}Y_{0.1}O_{3-\delta}$ (BCFZY) and $BaCo_{0.4}Fe_{0.4}Ce_{0.1}Y_{0.1}O_{3-\delta}$ (BCFCY) powders, illustrating that the cathode materials are pure phase with the same crystal structure as standard $BaCo_{0.4}Fe_{0.6}O_{2.73}$ (PDF-04-017-5204). Rietveld refinement of BCFZY and BCFCY cathodes (Fig. 2 (b-c)) illustrates they both have $Pm\bar{3}m$ space groups with lattice parameter of 4.109 Å and 4.127 Å, respectively. The R_{wp} values are 7.16% and 9.00%, meaning the calculations have a high level of fitness.

TGA of BZCYYb electrolytes

Fig. S1 shows the TGA data for the three electrolytes. As explained before, the first heating cycle was for removal of absorbed water (or dehydration) while in the second heating cycle, all weight loss of the electrolyte powder could be attributed to oxygen loss. Fig. 3 shows how oxygen content, calculated from the TGA data, changes with temperature. As expected, all three electrolytes have the same tendency to lose oxygen when heated up; the higher the Ce concentration, the more oxygen loss especially at high temperatures of ~800 ºC, and the data is close to literature[20].

Microstructure of symmetrical cells

The microstructure of the three proton conducting electrolytes (Ce-rich, ZrCe-bal and Zr-rich) after sintering is shown in Fig. 4 (a-c). From the top view, the surface appears dense for all three electrolytes, but there are some differences: The higher the Ce concentration, the larger the grain size of the BZCYYb electrolyte. Since the electrolyte powder synthesis and pellet sintering processes were the same, the difference in morphology is attributed to the Ce/Zr ratio: it is known that the $BaZrO_3$ has a higher melting temperatures and is more stable than $BaCeO_3$[22]. Fig. 4 (d-f) shows the cross-sections of the three symmetrical cells based on

the same BCFZY cathode over those three electrolytes. All three electrolytes are near fully dense, while the cathodes are porous with grain size < 1 μm and thickness of ~15-20 μm.

Electrochemical behaviors of symmetrical cells

Fig. 5 (a-c) shows the impedance spectra for a BCFZY/Ce-rich/BCFZY symmetrical cell in dry simulated air (< 5 ppm H_2O & CO_2 per Airgas, actual concentration might be higher) as well as moist air (3% H_2O) at 650, 550, and 450 ^oC. Both ohmic resistance R_Ω (from the high frequency intercept in the EIS spectra) and electrode apparent interfacial resistance R_{ai} (from the difference between the high frequency and low frequency intercepts in the EIS spectra) decreased when introducing H_2O. Fig. 6 (a-c) shows the results for the BCFZY/ZrCe-bal/BCFZY symmetrical cell under the same conditions. For this system, R_Ω decreased when introducing H_2O, while R_{ai} stayed almost the same at 550 ^oC and below (it increased slightly at 650 ^oC). Fig. 7 (a-c) is for the BCFZY/Zr-rich/BCFZY symmetrical cell. R_Ω follows the same trend as the other two, but introducing H_2O caused R_{ai} to increase. In Fig. 7(b-c), the dash line represents the fitting data of the EIS curve using Z-view. In the fitting, the high frequency part was ignored since it presents the grain boundary effect instead of the cell resistance.

- Changes in ohmic resistance R_Ω

Fig. 8(a) summarizes ohmic resistance R_Ω vs. inverse temperature for all three types of symmetrical cells in both simulated air and 3% moist air. Note that, first, as Ce concentration in the BZCYYb electrolyte increases, R_Ω decreases, meaning increase in bulk ionic conductivity. In fact, from the plot, $\sigma_{\mathrm{Ce-rich}} \approx 2\,\sigma_{\mathrm{ZrCe-bal}} \approx 4\,\sigma_{\mathrm{Zr-rich}}$ in the temperature range of ~450-650^oC. Such an observation is consistent with literature [8] showing Ce-rich electrolytes for Ba-based electrolytes tend to give higher ionic conductivity than Zr-rich electrolytes. It is also consistent with the oxygen contents determined from TGA (see Fig 3), showing the Ce-rich electrolyte has lower oxygen content, i.e., higher oxygen vacancy concentration, than the ZrCe-bal and Zr-rich electrolytes at elevated temperature (e.g., 550^oC). A second observation is that, upon introducing moisture, R_Ω dropped for all three electrolytes. The drop in R_Ω is attributed to the hydration reaction of water combining with oxygen vacancy (from Y and Yb acceptor doping) to form protons $(OH)_O^\bullet$:

$$H_2O + V_O^{\bullet\bullet} + O_O^\times \leftrightarrow 2\,(OH)_O^\bullet \qquad (1)$$

leading to higher bulk conductivity of the electrolyte, and it is well known for proton conducting oxide electrolytes.

- Changes in apparent interfacial resistance R_{ai}

Fig. 8 (b-d) summarizes cathode apparent interfacial resistance R_{ai} vs. inverse temperature for each of the three types of symmetrical cells. It should be noted that for proton conducting electrolytes such as BZCYYb that display mixed ionic and electronic conduction in air, R_{ai} – the difference between the high frequency and low frequency intercepts in an EIS spectrum is only an approximation for the actual cathode interfacial resistance R_i. This is due to electronic leakage through the proton conducting electrolyte, especially in dry air, that tends to make the measured apparent interfacial resistance appear smaller than the actual value, i.e., $R_{ai} < R_i$. Researchers have developed equations that help calculate the actual

interfacial resistance R_i [23,24]. However, these calculations are all based on assumptions about certain parameters such as electronic and ionic transport numbers (t_e and t_i) for the electrolyte in the interested temperature range. Without reliable experimental or theoretical t_e or t_i values for current materials, any estimation or correction based on those equations would be highly arbitrary and does not improve the accuracy of the analysis. As a result, in this study, R_{ai} was used directly as a first approximation of the electrode activity.

Nevertheless, in dry simulated air, the BCFZY cathode shows comparable R_{ai} among all three types of symmetrical cells, despite the difference in BZCYYb electrolytes with varying Ce/Zr ratios. This is understandable due to the same cathode material and processing condition. This also indicates that the oxygen reduction reaction (ORR) is unlikely to be limited by the bulk ionic conductivity of the electrolytes.

However, upon H_2O introduction, as mentioned before, the cathode symmetrical cells behave very differently: apparent interfacial resistance R_{ai} increased over the Zr-rich electrolyte, but decreased over the Ce-rich electrolyte, while staying the same over the ZrCe-bal electrolyte.

As to the behavior of increasing cathode R_{ai} upon moisture introduction for the BCFZY/Zr-rich/BCFZY symmetrical cell (Figs. 7 and 8(d)), similar observation has been made by other researcher[1] as well as for other cathodes such as LSCF and BSCF[15], though most are not triple conducting cathodes and the electrolyte used were mostly Ce-rich BZCYYb electrolyte[19,25]. One earlier explanation is that moisture addition to air might lead to strong adsorption of H_2O on the cathode (and electrolyte) surface, which blocks ORR reaction site. However, the triple conducting nature of the BCFZY cathode means the entire cathode surface would be active for ORR and a low percentage of moisture is not expected to impact much.

Therefore, a more likely explanation is related to the depletion of electron hole by the defect reaction in the electrolyte between electron holes, water vapor, and lattice oxygen ($O_O\times$) to form protons (or protonated oxygen) while releasing oxygen gas, as below:

$$4\,h^{\bullet} + 4\,O_O^{\times} + 2\,H_2O_{(g)} \leftrightarrow 4(OH)_O^{\bullet} + O_2\,, \qquad (2)$$

Introducing moisture would shift the above reaction to the right side, leading to a drop in hole concentration[26]. The result will be higher electronic resistance through the electrolyte and less electronic leakage. This would increase the ionic transport number t_i of the electrolyte toward unity, which, in turn, would lead to higher electrode apparent interfacial resistance R_{ai}, as observed in Fig. 7 and 8(d).

On the other hand, the behavior of decreasing R_{ai} with moisture introduction for the BCFZY/Ce-rich/BCFZY symmetrical cell is also interesting. There have been similar observations on alternative cathodes such as $Ba_{0.95}La_{0.02}Fe_{0.8}Zn_{0.2}O_{3-\delta}$[27] and $Pr_2NiO_{4+\delta}$[28]. The exact reason for reducing R_{ai} upon moisture introduction in these symmetrical cells is not clear at this moment. As mentioned before, the hydration of the proton conducting electrolyte in air would suppress electronic leakage, which should lead to increase in R_{ai}.

One possible explanation for the observed reduction in R_{ai} is about the greater availability of H_2O molecules for the ORR over proton conducting electrolytes:

$$O_2 + 4\,(OH)_O^{\bullet} + 4e' \leftrightarrow 2\,H_2O_{(g)} + 4\,O_O^{\times}, \qquad (3)$$

especially for the reverse (half-cell) reaction from water and lattice oxygen $O_O^{\times}$ to protons. Since EIS for a cathode symmetrical cell is obtained under zero bias condition, when there

are very few H_2O molecules, as in dry simulated air, the reverse of reaction (3) from H_2O and lattice oxygen $O_O^{\times}$ to protons, despite the low AC bias, might be limited due to the near absence of H_2O. Introducing moisture would naturally alleviate the problem of "starvation" or inadequacy of H_2O as a reactant, accelerate the reverse of reaction (3), and, possibly, decrease R_{ai} in EIS measurements.

An alternative explanation is that ORR in dry simulated air over the Ce-rich electrolyte (or any proton conducting electrolytes) would follow a different route involving only oxygen vacancy and no proton, as below:

$$O_2 + 2\,V_O^{\bullet\bullet} + 4e' \leftrightarrow 2\,O_O^{\times}, \quad (4)$$

After introducing moisture, ORR might change, maybe partially, to the route involving protons (i.e., reaction (3)). The kinetics for ORR by the proton route (reaction (3)) might be faster than the oxygen vacancy route (reaction (4)), leading to a large drop in R_{ai} in EIS measurements.

Either way, for Ce-rich electrolyte, the effect of moisture on electrode kinetics is hypothesized to be large enough to overcome the effect from reduced electronic leakage, and overall R_{ai} drop upon introducing moisture.

Interactions between BCFZY cathode and BZCYYb electrolytes

However, despite the above hypotheses, there are questions still unanswered, especially about why the same BCFZY cathode behaved differently (i.e., R_{ai} responses to moisture) over different BZCYYb electrolytes, all of which supposed to be proton conducting. To understand this, as stated, the interactions between the BCFZY cathode and the three electrolytes had been studied, and the results are presented below.

- XRD for cathode/electrolyte mixed powders

Fig. 9 (a-c) show XRD Rietveld refinement of three mixtures, each contained BCFZY cathode and one of the three BZCYYb electrolytes at a weight ratio of 1:1 and had gone through heat treatment at 1100 ^{o}C for 4 h. The unit cell volume of the BCFZY cathode after the heat treatment was 70.70, 70.21, 69.90 $Å^3$ when mixed with Ce-rich, ZrCe-bal, Zr-rich electrolyte, respectively. As shown in Fig. 9 (d), the unit cell volume of BCFZY cathode in all three mixtures were all larger than the as-synthesized sample (69.57 $Å^3$). This is because under the cathode firing process at 1100 ^{o}C, there would be mutual diffusion between the cathode and the electrolyte. The larger high-concentration B-site elements such as Ce and Zr in the electrolyte would diffuse into the cathode and expand its lattice. In addition, it is observed that the higher the electrolyte Ce concentration, the greater the cathode volume expansion after firing (see Fig. 9(d)). Such a phenomenon can be understood in two aspects. Firstly, Ce ion is larger than Zr ion. Secondly, Ce should have greater tendency to diffuse than Zr given $BaCeO_3$ is known to have lower melting temperature and stability than $BaZrO_3$ [22]. (The reason for focusing only on the cathode unit cell volume change is that the electrolytes with different Ce/Zr ratios have different crystal structures from cubic to orthorhombic, which would complicate the comparison between samples.)

- EDS line scan for the cathode/electrolyte interface

Fig. 10 (a-c) shows EDS line scans along the cross-sections for three representative symmetrical cells: BCFZY/Ce-rich/BCFZY, BCFZY/ZrCe-bal/BCFZY, and BCFZY/Zr-

rich/BCFZY, respectively. The origin or "0" in the horizontal "distance" axis corresponds to the interface between the BCFZY cathode and BZCYYb electrolyte. (Only data from the dense electrolyte side are presented. This is due to the large difference in porosity between the porous cathode and the dense electrolyte leading to a large gap of signal intensity at the interface.) Fig. 10 (a) is for the cell with Ce-rich electrolyte. Within ~1 μm from the interface into the dense electrolyte, the intensity of Ce gradually increases, while the intensity of Co and Fe decreases. It means that Ce in the bulk of electrolyte was lost due to diffusion into the cathode, while Co and Fe in the BCFZY cathode diffused into the electrolyte. By contrast, in Fig. 10 (b-c), the intensity change for either Zr or Co/Fe around the cathode/electrolyte interface is much less obvious, illustrating the ZrCe-bal and Zr-rich electrolytes with a cubic structure are more stable than the Ce-rich electrolyte with an orthorhombic structure and there was much less interdiffusion involved. It should be mentioned that the trends in EDS line scan about Ce/Co/Fe intensity were repeatable over multiple regions across multiple samples, indicating the validity of the observations.

- Test of Ce-containing BCFCY cathode over Zr-rich electrolyte

To explain why introducing moisture caused the same BCFZY cathode to display decreasing apparent interfacial resistance R_{ai} over the Zr-rich electrolyte but increasing R_{ai} over the Ce-rich electrolyte, we further hypothesize that Ce doping into the Ze-containing BCFZY cathode would enhance proton conduction in the cathode, while neat BCFZY, though active in dry air, has limited proton conduction capability. In addition, previous studies also show Ce-rich proton conducting electrolytes tend have higher ionic transport number t_i than Hf-rich ones, which are expected to behave very similarly to Zr-rich electrolytes due to similarity between Zr and Hf [29–31]. This means the Zr-rich BZCYYb electrolyte would have greater electronic leakage, while the Ce-rich electrolyte would be less influenced.

Therefore, on the Zr-rich electrolyte with slightly lower t_i, the limited proton conduction in the BCFZY cathode means ORR would largely be limited to the triple phase boundary region. Despite the greater availability of H_2O molecules and potentially faster ORR for the proton route (reaction (3)), the effect of introducing moisture might be dominated by (i) water suppressing electronic leakage, and (ii) limited ORR proceeding via the proton route. These two effects lead to the observations of higher R_{ai} with introducing moisture, as in Fig. 7 and 8(d).

In comparison, on the Ce-rich electrolyte, it is less impacted by electronic leakage due to higher t_i. Meanwhile, due to extensive Ce diffusion into the BCFZY cathode, when moisture is introduced, the cathode, at least near the interface, conducts proton better and the sites for faster ORR via the proton route might greatly expand. As a result, R_{ai} decreases upon moisture introduction.

For the ZrCe-bal electrolyte, the two effects (water suppressing electronic leakage causing R_{ai} to increase vs. promoting ORR via the proton route causing R_{ai} to drop) might roughly balance each other. Therefore, no obvious change in R_{ai} was observed.

To test the hypothesis that Ce doping into BCFZY cathode might enhance proton conduction and cathode activity, especially in humidified air, a related cathode $BaCo_{0.4}Fe_{0.4}Ce_{0.1}Y_{0.1}O_{3-\delta}$ (BCFCY) is synthesized by replacing all Zr (in BCFZY) with Ce. Fig. 11 shows the impedance spectra for such a BCFCY/Zr-rich/BCFCY symmetrical cell in

both simulated air and moist air (3% H_2O) at 650 °C. Ohmic resistance R_Ω of the Ce-containing BCFCY symmetrical cell in both atmospheres were close to the Zr-containing symmetrical cell, which is expected from the same Zr-rich electrolyte composition and geometry. After introducing 3% H_2O, the new Ce-containing BCFCY cathode does show reduction in R_{ai} at 650 °C, as opposed to increasing R_{ai} for the Zr-containing BCFZY cathode (see Fig. 7(a) and 8(d)). This seems to confirm that Ce doping to this BaCoFeO-type cathode might promote proton conduction in the cathode and improve the activity upon introducing moisture, even over the Zr-rich electrolyte.

Finally, it should be mentioned that all the above analyses only constitute simplified frameworks that serve as a starting point for further understanding. There are many questions that remain unanswered for such BaCoFe-type cathodes over BZCYYb proton conducting electrolytes and there might be alternative explanations. Future studies including detailed materials characterizations, ab initial calculation (e.g., by the density functional theory or DFT method), as well as electrochemical modeling are needed to fully understand conductivity of BCFZY/BCFCY cathodes in different atmospheres, their water permeation rates, ionic transport numbers for different BZCYYb electrolytes, as well as many of the observed complex electrochemical behaviors.

Conclusions

This study compares the behaviors of $BaCo_{0.4}Fe_{0.4}Zr_{0.1}Y_{0.1}O_{3-\delta}$ (BCFZY) cathode over $BaZr_{0.8-x}Ce_xY_{0.1}Yb_{0.1}O_{3-\delta}$ (BZCYYb) electrolytes with different Ce/Zr ratios (i.e., x = 0.1, 0.4, and 0.7). Consistent with expectation, for the BZCYYb electrolytes, the higher the Ce concentration, the bigger the grain size in sintered pellet and more oxygen vacancy, leading to higher conductivity especially at high temperature (e.g., 550 °C). Furthermore, the comparable BCFZY cathode apparent interfacial resistance R_{ai} over the three different electrolytes in dry simulated air suggests that the cathode oxygen reduction reaction is limited by oxygen adsorption/dissociation process instead of the ionic conductivity of the electrolyte. After introducing ~3% moisture to air, cathode R_{ai} drops for the symmetrical cell with Ce-rich electrolyte, while it increases for the Zr-rich electrolyte. Analyses such as EDS line scanning at the cathode/electrolyte interfaces and XRD Rietveld refinement comparing the cathode's unit cell volume change when fired together with different BZCYYb electrolytes suggest that Ce has a stronger tendency than Zr to diffuse from the electrolyte to the cathode. And the diffused Ce likely increases the BCFZY cathode activity. Such a hypothesis is supported by the observation that replacing all Zr by Ce in the BaCoFeO-type cathode over the Zr-rich electrolyte also increases the cathode activity upon moisture introduction at 650 °C. Additional experiments and theoretical calculations will be carried out in the future to fully understand such phenomenon.

Acknowledgments

This research is supported by the National Science Foundation (Award No. DMR-1848305). The use of facilities at FIU Advanced Materials Engineering Research Institute (AMERI) is acknowledged.

References

1. C. Duan et al., *Science*, **349**, 1321–1326 (2015).

2. E. D. Wachsman and K. T. Lee, *Science*, **334**, 935–939 (2011).

3. A. P. Tarutin, J. G. Lyagaeva, D. A. Medvedev, L. Bi, and A. A. Yaremchenko, *J. Mater. Chem. A*, **9**, 154–195 (2021).

4. L. Yang et al., *Science*, **326**, 126–129 (2009).

5. Y. Xu et al., *Sep. Purif. Technol.*, **297**, 121482 (2022).

6. S. Sun and Z. Cheng, *J. Electrochem. Soc.*, **165**, F836–F844 (2018).

7. K. Bae, D. H. Kim, H. J. Choi, J.-W. Son, and J. H. Shim, *Adv. Energy Mater.*, **8**, 1801315 (2018).

8. Y. Guo, Y. Lin, R. Ran, and Z. Shao, *J. Power Sources*, **193**, 400–407 (2009).

9. K. Bae et al., *Nat. Commun.*, **8**, 14553 (2017).

10. H. Shimada et al., *J. Electrochem. Soc.*, **168**, 124504 (2021).

11. Y. Zhou et al., *Adv. Funct. Mater.*, **31**, 2105386 (2021).

12. K. Yang et al., *Ceram. Int.*, **40**, 15073–15081 (2014).

13. S. Choi et al., *Nat. Energy*, **3**, 202–210 (2018).

14. S. Sun and Z. Cheng, *J. Electrochem. Soc.*, **167**, 024514 (2020).

15. S. Sun and Z. Cheng, *J. Electrochem. Soc.*, **164**, F3104–F3113 (2017).

16. L. Fan and P.-C. Su, *J. Power Sources*, **306**, 369–377 (2016).

17. Y. Meng et al., *Solid State Ion.*, **368**, 115639 (2021).

18. J.-W. Jhuang et al., *Int. J. Hydrog. Energy*, **46**, 9767–9774 (2021).

19. S. I. Sozal et al., *N T E R N T O N J O U R N O F H R O G E N E N E R G*, 11.

20. Y. Zhang et al., *Asia-Pac. J. Chem. Eng.*, **14** (2019) https://onlinelibrary.wiley.com/doi/10.1002/apj.2322.

21. A. VahidMohammadi and Z. Cheng, *J. Electrochem. Soc.*, **162**, F803–F811 (2015).

22. S. Yamanaka et al., *J. Alloys Compd.* (2003).

23. D. Poetzsch, R. Merkle, and J. Maier, *J. Power Sources*, **242**, 784–789 (2013).

24. R. Strandbakke et al., *Solid State Ion.*, **278**, 120–132 (2015).

25. Y. Chen et al., *J. Power Sources*, **440**, 227122 (2019).

26. H. Taherparvar, *Solid State Ion.*, **162–163**, 297–303 (2003).

27. Z. Wang et al., *Ceram. Int.*, **46**, 18216–18223 (2020).

28. A. Grimaud et al., *J. Electrochem. Soc.*, **159**, B683–B694 (2012).

29. L. Lei et al., *Energy Convers. Manag.*, **218**, 113044 (2020).

30. R. J. Murphy, dissertation, Georgia Institute of Technology, Atlanta, GA (2019).

31. R. Murphy et al., *Adv. Funct. Mater.*, **30**, 2002265 (2020).

Figure Captions

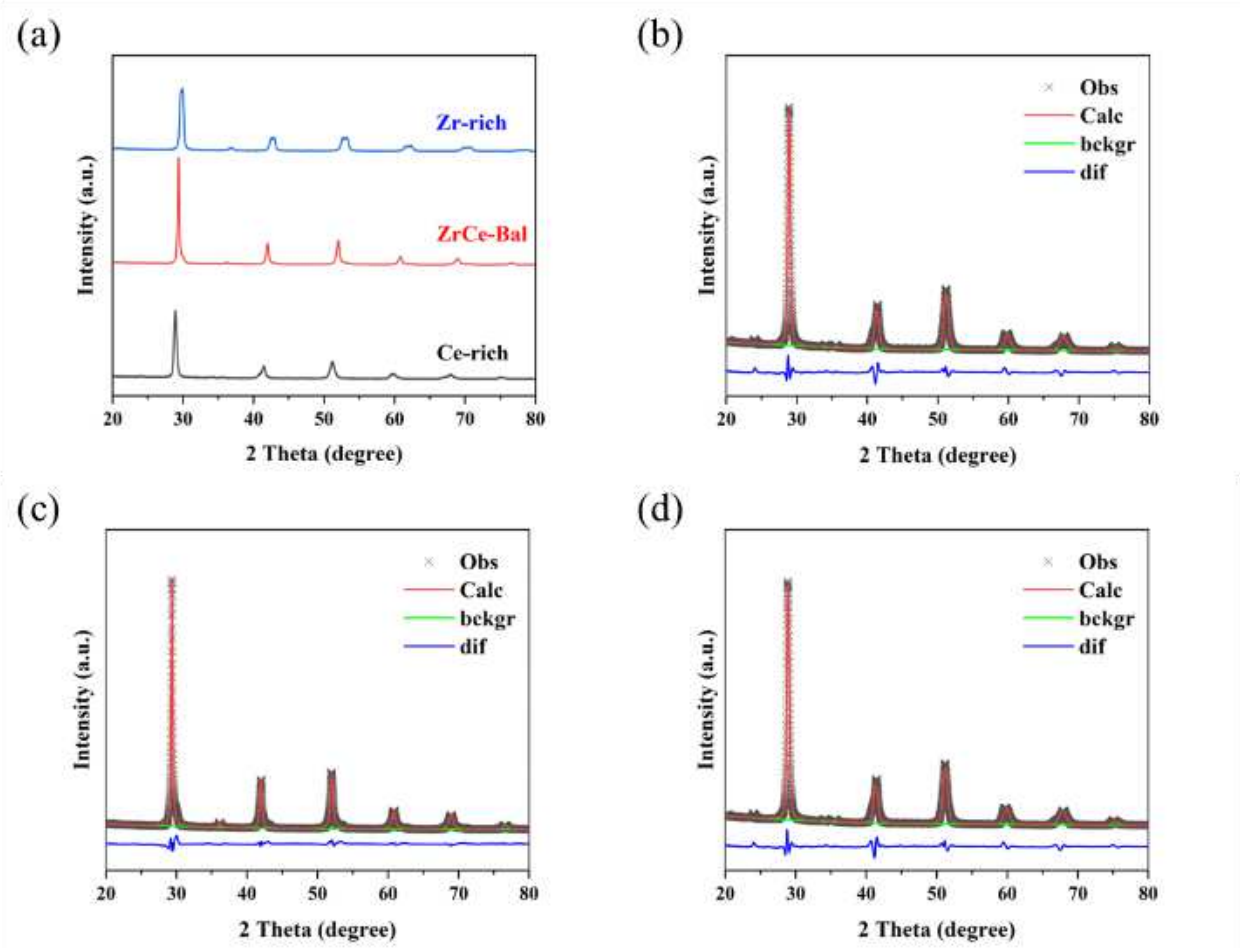

Fig. 1 (a) XRD patterns and (b-d) XRD Rietveld refinement for the three electrolyte powders after heat treatment at 1300 ºC for 5 h, note that (b) is for $BaZr_{0.1}Ce_{0.7}Y_{0.1}Yb_{0.1}O_{3-\delta}$ (Ce-rich), (c) for $BaZr_{0.4}Ce_{0.4}Y_{0.1}Yb_{0.1}O_{3-\delta}$ (ZrCe-bal), and (d) for $BaZr_{0.7}Ce_{0.1}Y_{0.1}Yb_{0.1}O_{3-\delta}$ (Zr-rich).

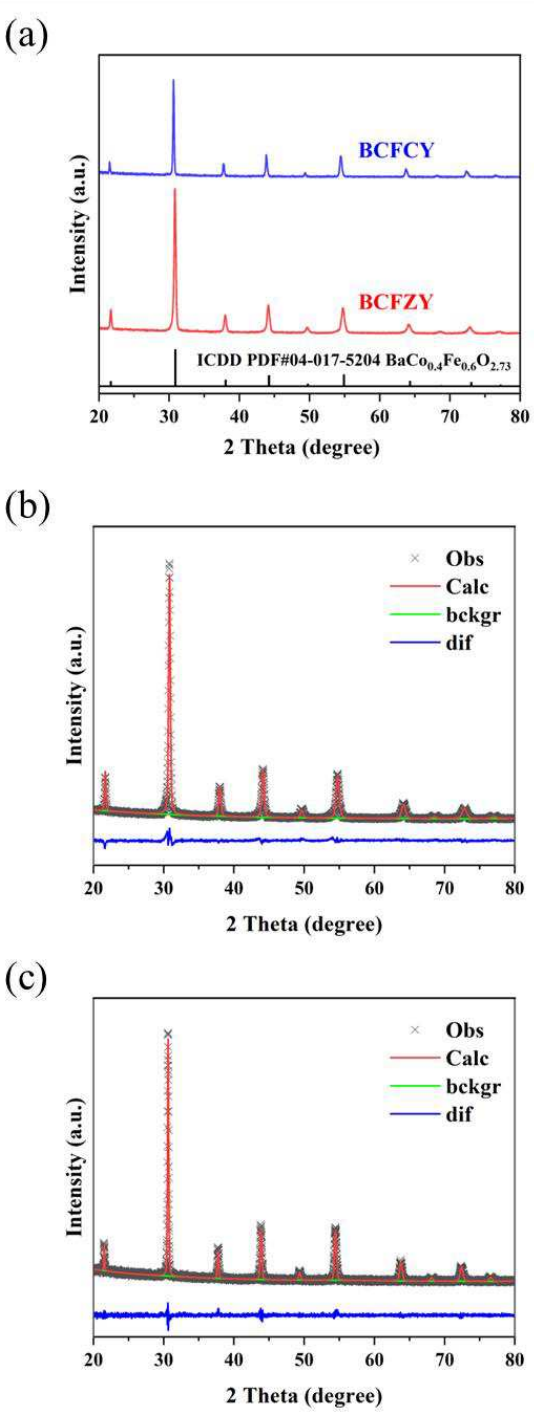

Fig. 2 (a) XRD patterns of $BaCo_{0.4}Fe_{0.4}Zr_{0.1}Y_{0.1}O_{3-\delta}$ (BCFZY) and $BaCo_{0.4}Fe_{0.4}Ce_{0.1}Y_{0.1}O_{3-\delta}$ (BCFCY) cathodes overlaid with the pattern for $BaCo_{0.4}Fe_{0.6}O_{2.73}$ (PDF-04-017-5204); (b and c) Rietveld refinement of (b) BCFZY powder after firing at 1000 ºC for 5 h and (c) BCFCY powder after firing at 1200 ºC for 5 h.

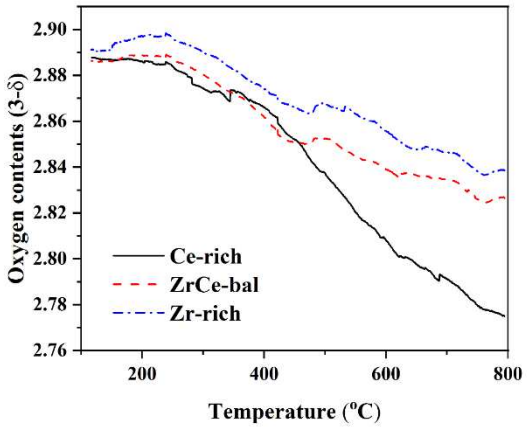

Fig. 3 Oxygen contents of the three BZCYYb electrolytes. As stated, all data were from the second heating/cooling cycle, while the adsorbed water was removed in the first heating/cooling cycle.

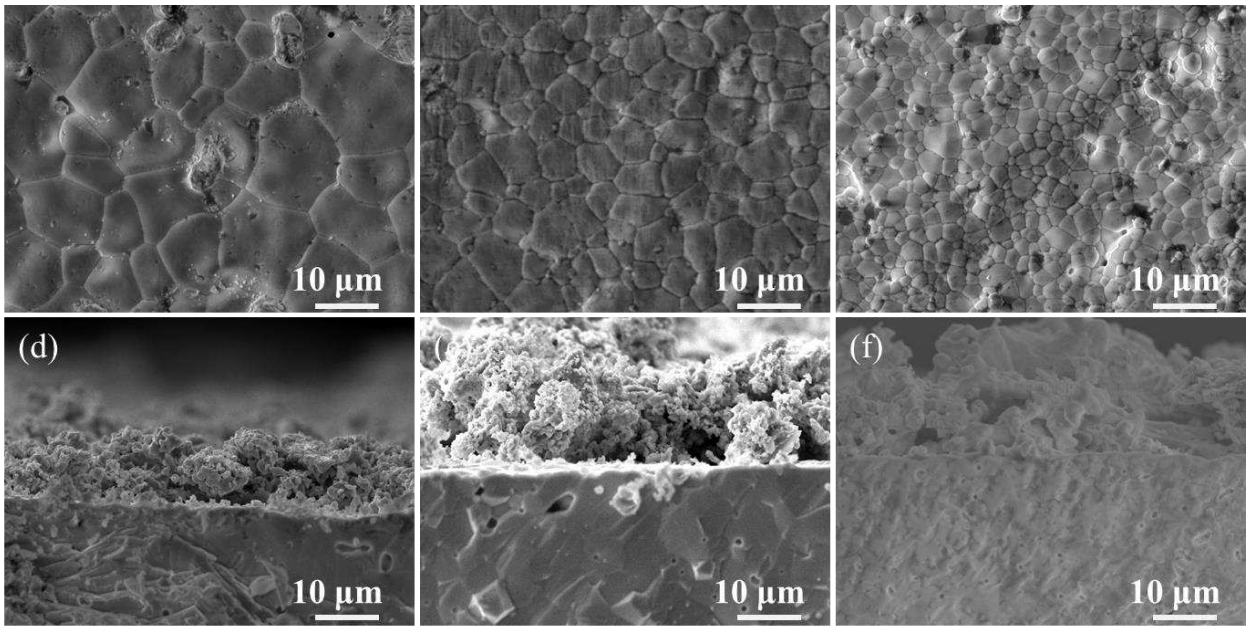

Fig. 4 (a-c) SEM images showing the top surfaces for the three electrolytes: (a) Ce-rich, (b) ZrCe-bal, (c) Zr-rich; (d-f) SEM images showing the cross-sections of the three types of cathode symmetrical cells: (d) BCFZY/Ce-rich/BCFZY, (e) BCFZY/ZrCe-bal/BCFZY, (f) BCFZY/Zr-rich/BCFZY.

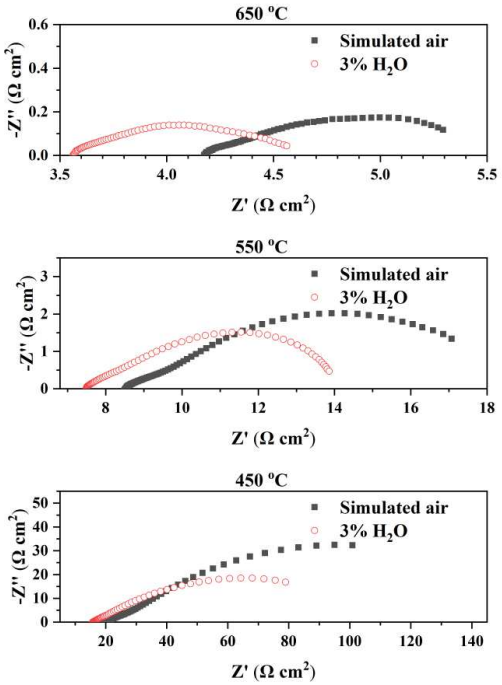

Fig. 5 Impedance spectra for a BCFZY/Ce-rich/BCFZY symmetrical cell in dry simulated air (<5 ppm H_2O and CO_2 by volume) versus moist air (3% H_2O by volume) at (a) 650 °C, (b) 550 °C, (c) 450 °C. Note the apparent interfacial resistance R_{ai} decreases upon H_2O introduction, especially at lower temperature.

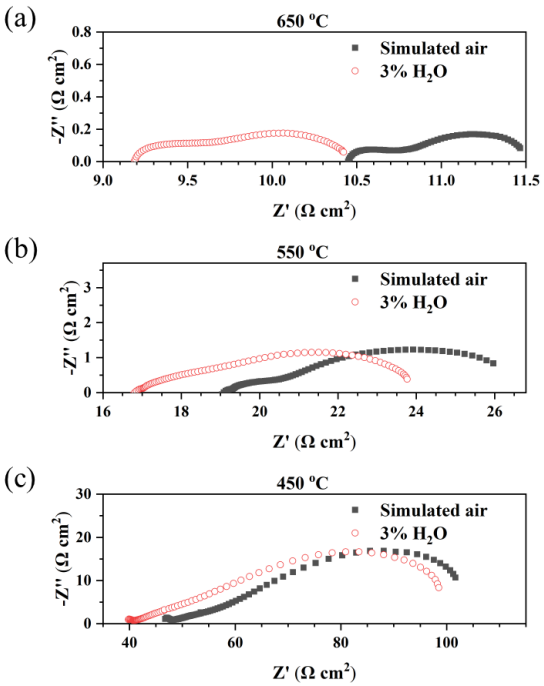

Fig. 6 Impedance spectra for a BCFZY/ZrCe-bal/BCFZY symmetrical cell in dry simulated air (<5ppm H_2O and CO_2 by volume) versus moist air (3% H_2O by volume) at (a) 650 °C, (b) 550 °C, (c) 450 °C. Note the apparent interfacial resistance R_{ai} stays roughly the same upon H_2O introduction.

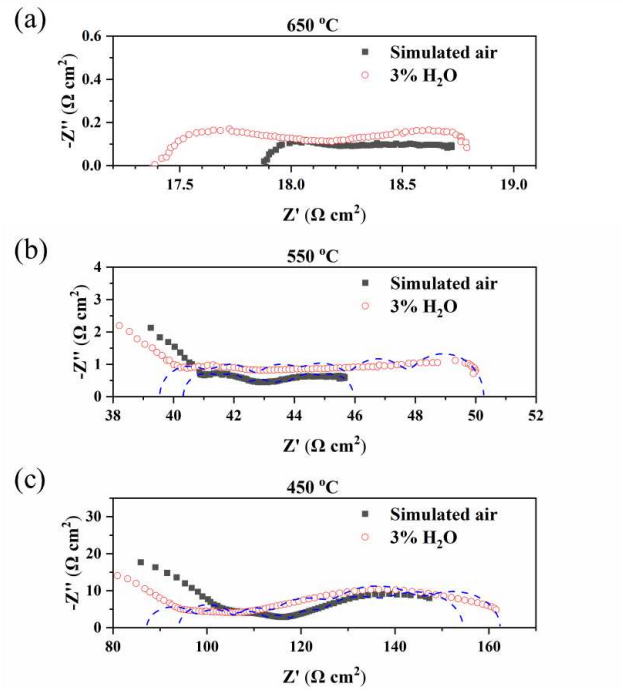

Fig. 7 Impedance spectra for a BCFZY/Zr-rich/BCFZY symmetrical cell in dry simulated air (<5ppm H_2O and CO_2 by volume) versus moist air (3% H_2O by volume) at (a) 650 °C, (b) 550 °C, (c) 450 °C. Note the apparent interfacial resistance R_{ai} increases upon H_2O introduction.

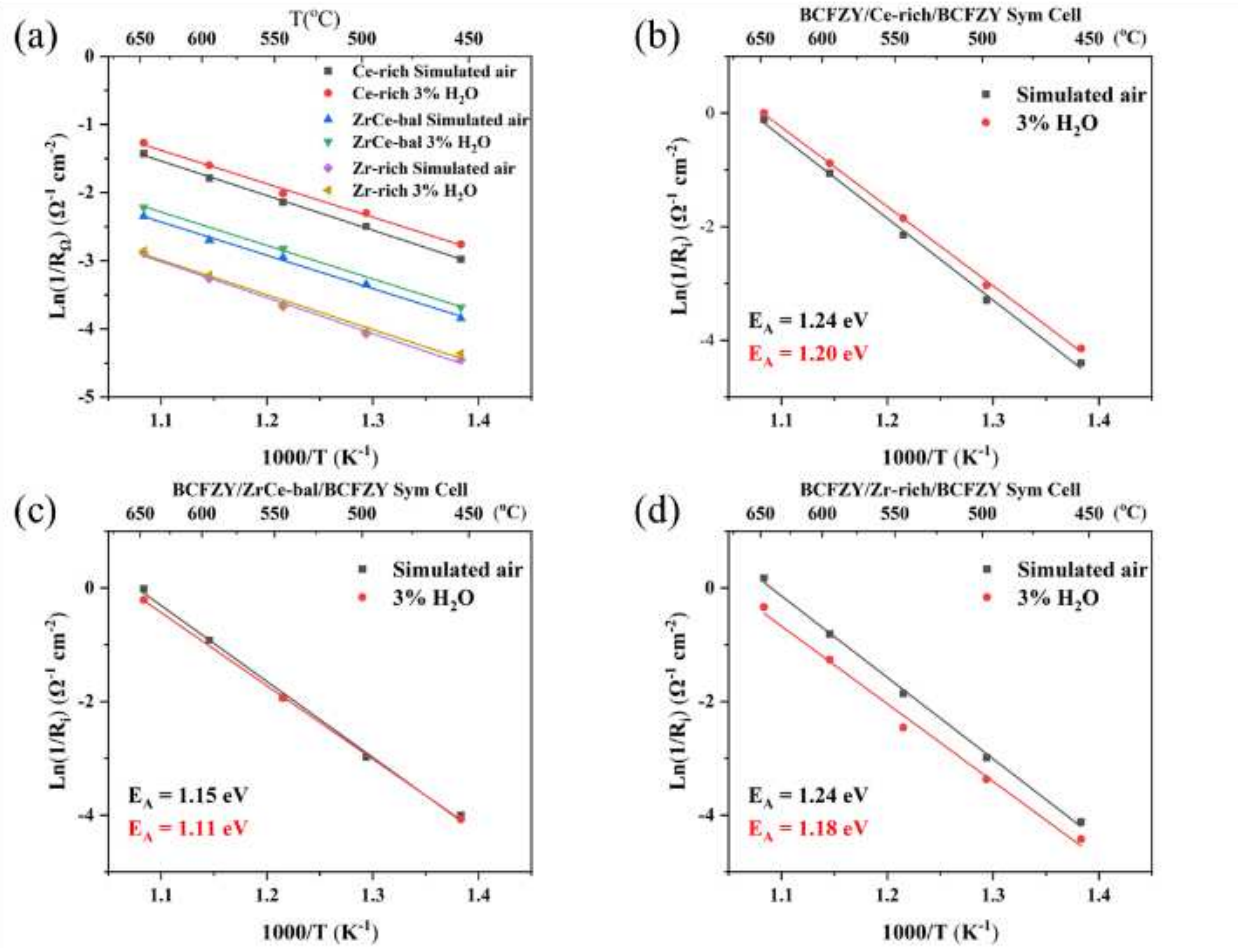

Fig. 8 (a) Ohmic resistance (R_Ω) vs. inverse temperature for three types of symmetrical cells in simulated air and 3% H_2O moist air; (b-d) Apparent interfacial resistance (R_{ai}) vs. inverse temperature with corresponding activation energy in both simulated air and 3% H_2O moist air for three types of symmetrical cells: (b) BCFZY/Ce-rich/BCFZY (c) BCFZY/ZrCe-bal/BCFZY (d) BCFZY/Zr-rich/BCFZY.

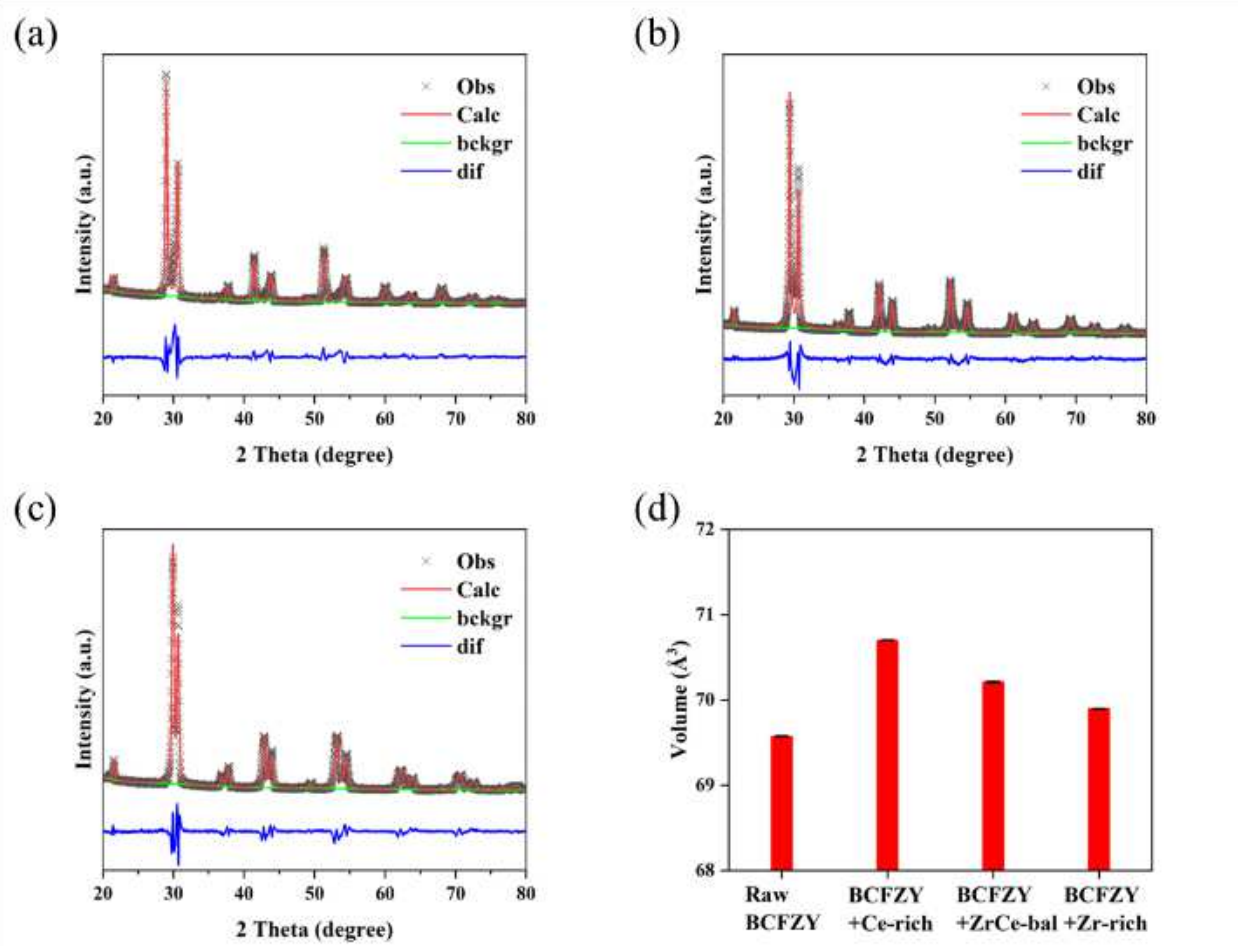

Fig. 9 XRD Rietveld refinement of BCFZY cathode and BZCYYb electrolyte mixed samples (a) BCFZY+Ce-rich (b) BCFZY+ZrCe-bal (c) BCFZY+Zr-rich (d) the volume of BCFZY cathode before and after sintering with different electrolytes (error bar too small to show).

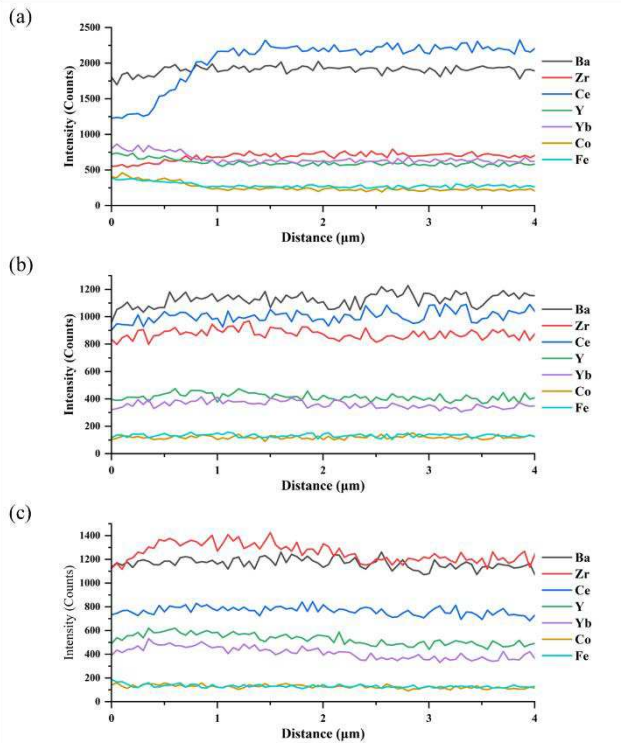

Fig. 10 EDS line scans of cross-sections of three symmetrical cells with the focus on the cathode/electrolyte interface: (a) BCFZY/Ce-rich/BCFZY (b) BCFZY/ZrCe-bal/BCFZY (c) BCFZY/Zr-rich/BCFZY.

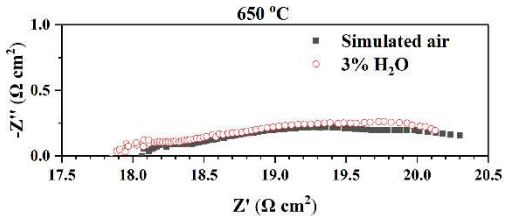

Fig. 11 Impedance spectra for a BCFCY/Zr-rich/BCFCY symmetrical cell in dry simulated air (<5 ppm H_2O and CO_2 by volume) versus moist air (3% H_2O)

Supplementary Material for publication in the Electronic Edition is Optional - Limited to ONE file of three pages or less **or** ONE Video file

Title: $BaCo_{0.4}Fe_{0.4}Zr_{0.1}Y_{0.1}O_{3-\sigma}$ Cathode Performance for Proton Conducting Solid Oxide Fuel Cells with $BaZr_{0.8-x}Ce_xY_{0.1}Yb_{0.1}O_{3-\delta}$ Electrolytes

Supplementary Material:

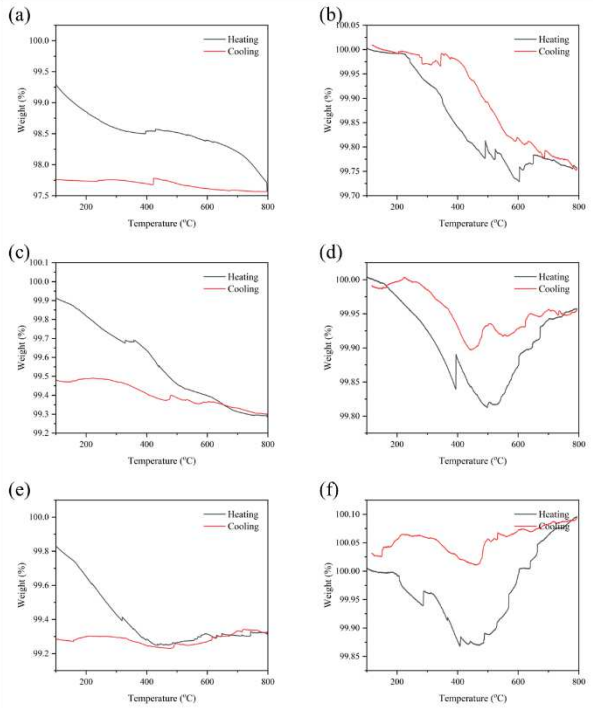

Fig.S1 TGA data for BZCYYb electrolyte powders (a) Ce-rich 1st cycle, (b) Ce-rich 2nd cycle, (c) ZrCe-bal 1st cycle, (d) ZrCe-bal 2nd cycle, (e) Zr-rich 1st cycle, (f) Zr-rich 2nd cycle.